Journal of Systems Engineering and Electronics
Vol. 28, No. 3, June 2017, pp.472 – 480

Micro-motion dynamics analysis of ballistic targets based on infrared detection

Junliang Liu[1,*], Yanfang Li[2], Shangfeng Chen[1], Huanzhang Lu[1], and Bendong Zhao[1]

1. College of Electronic Science and Engineering, National University of Defense Technology, Changsha 410073, China;
2. Beijing Institute of Remote Sensing Equipment, Beijing 100854, China

Abstract: The dynamic characteristics related to micro-motions, such as mechanical vibration or rotation, play an essential role in classifying and recognizing ballistic targets in the midcourse, and recent researches explore ways of extracting the micro-motion features from radar signals of ballistic targets. In this paper, we focus on how to investigate the micro-motion dynamic characteristics of the ballistic targets from the signals based on infrared (IR) detection, which is mainly achieved by analyzing the periodic fluctuation characteristics of the target IR irradiance intensity signatures. Simulation experiments demonstrate that the periodic characteristics of IR signatures can be used to distinguish different micro-motion types and estimate related parameters. Consequently, this is possible to determine the micro-motion dynamics of ballistic targets based on IR detection.

Keywords: micro-motion dynamics, infrared (IR) signatures, target recognition, parameters estimation.

DOI: 10.21629/JSEE.2017.03.07

1. Introduction

Since types of ballistic targets including reentry vehicles (RV), boosters, decoys and separation debris group closely in space and share the same trajectory and velocity in the midcourse flight, it is very difficult to distinguish them using the available information of bulk motion [1]. However, separated targets are always in vibrational or rotational motions (referred to as micro-motions), such as spinning, precession and tumbling, in addition to their bulk motions [2]. Thus, the micro-motion characteristics of ballistic targets become significant clues to discriminate RV from decoys and other missile parts.

In recent years, research of micro-motion dynamics of ballistic targets in the field of radar has proliferated [3]. The main methods of studying target micro-motion dynamics include radar micro-Doppler effects analysis and scattering characteristics analysis techniques [4,5]. (i) Micro-Doppler effects induced by micro-motion dynamics have been widely used to classify different ballistic targets. For example, Chen et al. derived formulas of micro-Doppler induced by several micro-motion types and analyzed time-varying micro-Doppler features using high-resolution transforms [4]. (ii) Radar scattering characteristics of ballistic targets have also been studied as important evidence to support ballistic target recognition. For example, Feng et al. extracted the micro-motion frequency from the radar cross-section (RCS) of ballistic targets for classification [5].

In the ballistic missile defense, the radar system is mainly used in the ground detection and pre-warning systems. While, for the detecting equipment onboard the missile, the radar is not suitable due to the limitations of space and cost. Generally the optical detection systems, such as the infrared (IR) detectors, are equipped on the interceptor to detect and recognize the true RVs [2].

IR detectors often work in the middle and terminal guidance phases. Due to long-distant detection, for example about 100 – 300 km away from IR sensor, even a large-size target always appears in a single pixel on the focal plane sensor array [6]. Thus the properties of the target could only be represented by the irradiance intensity signatures comprised of the total sensed energy with the IR sensors. It is found that the micro-motion dynamics of the targets would induce a periodic fluctuating variation on the IR signatures, and this periodic fluctuation comes from the periodic change of target geometrical projected area along the line-of-sight (LOS) of IR detectors. It is found that target projected area time series can reflect the characteristics of micro-motions and geometrical shape. Moreover, target projected area time series can be decoupled from IR signatures and derived as accurate mathematical formulas using micro-motion and shape parameters, which provides feasible theoretical basis to analyze target micro-motion characteristics.

Manuscript received March 02, 2016.
*Corresponding author.

In this paper, we investigate the ways of extracting micro-motion features of ballistic targets based on IR detection. This paper is structured as follows: Section 2 introduces two micro-motion types of ballistic targets, and derives the mathematical formulas of target projected area under the assumption of observed targets with conical shapes. In Section 3, the IR signature models of targets with micro-motions are developed. Given it, the component of periodic characteristics is effectively decoupled from original IR signatures using our proposed principle. In Section 4, according to the extracted periodic characteristics component, we design the algorithms to distinguish different types of micro-motions and estimate the micro-motion parameters.

2. Micro-motion types of ballistic targets

After burnout, the ballistic missile would release RVs and decoys, as well as disintegrate into debris. Since the true RVs are spin-stabilized, they would be in precession motion due to the separation disturbance and keep this motion until re-entering the atmosphere [3]. While, other missile parts usually tumble when affected by the disturbance moments.

2.1 Precession

After released, RV keeps its stability in flight by spinning rapidly. Due to the disturbance of lateral moments, RV will do precession around the target moving direction. Illustrated in Fig. 1 is a cone target with precession, where the semi-vertical angle and radius of the cone target are α and R respectively. The precession motion can be viewed as a combination of two types of rotational motions: (i) the target rotates around the angular moment vector $\boldsymbol{H}$, called coning motion. The angle between $\boldsymbol{e}_z$ and $\boldsymbol{H}$ is coning angle θ. (ii) the target spins along its fundamental inertia axis $\boldsymbol{e}_z$.

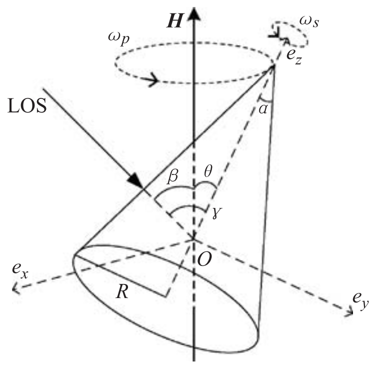

Fig. 1 Diagram of a cone target with precession

Assuming that the angular frequencies of coning motion and spinning are ω_p and ω_s respectively, the observation angle between the vertical axis of cone target and LOS can be represented as

$$\gamma(t) = \arccos(\cos\theta\cos\beta + \cos\omega_p t \sin\theta \sin\beta) \qquad (1)$$

where β is the angle between the LOS and $\boldsymbol{H}$. Because the vertical moment of an RV is greatly larger than its lateral moment due to rapid spinning motion, the angle θ is comparatively small, about $3° - 5°$. Thus, $\gamma(t)$ can be simplified as

$$\gamma(t) = \beta - \theta\cos\omega_p t.$$

For convenience, we denote the projected area of the cone target by $A_{proj}(R, \alpha, \gamma)$, as indicated in the shadow area of Fig. 2(a). We also define the cone surface area under the field of view of the IR sensor as $A_{cone}(R, \alpha, \gamma)$, which is shown in the gray region in Fig. 2(a).

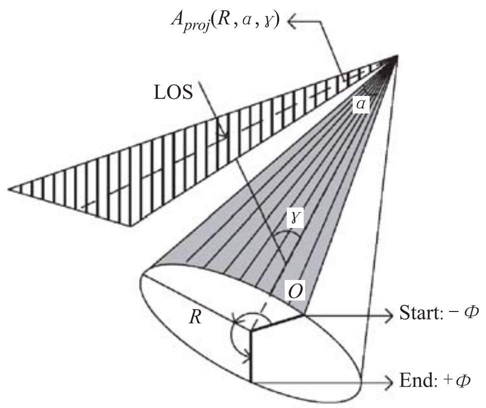

(a) Projection displaying of a cone target

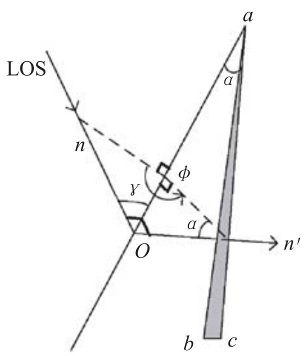

(b) Projection computing of a single patch

Fig. 2 Projecting diagram of a cone target along LOS

To compute the projected area of a cone target, a common method is to divide the target surface into a number of triangle patches, and sum all of patch projected areas along the LOS. As shown in Fig. 2(b), taking any piece of triangle patch Δabc as an example, its projected area can be expressed as

$$A^i_{proj}(R, \alpha, \gamma) = A_{\Delta abc}\cos(-\boldsymbol{n}, \boldsymbol{n}') =$$
$$A_{\Delta abc}[\cos\gamma\cos(\pi/2 - \alpha) + \cos\phi\sin\gamma\sin(\pi/2 - \alpha)] =$$
$$A_{\Delta abc}[\cos\gamma\sin\alpha + \cos\phi\sin\gamma\cos\alpha]$$

where $A_{\Delta abc}$ is the area of the triangle patch Δabc, $\boldsymbol{n}$ is the LOS vector, and $\boldsymbol{n}'$ denotes the normal vector of Δabc. As labeled in Fig. 2(b), assuming ϕ is the surface angle around the vertical axis of the target, thereof $A_{proj}(R, \alpha, \gamma)$ can be derived as

$$A_{proj}(R,\alpha,\gamma) = \int A^i_{proj}(R,\alpha,\gamma) =$$
$$\int_{-\Phi}^{\Phi} 1/2 \cdot R^2/\sin\alpha \cdot [\cos\gamma\sin\alpha + \cos\phi\sin\gamma\cos\alpha]\mathrm{d}\phi =$$
$$\int_{0}^{\Phi} R^2/\sin\alpha \cdot [\cos\gamma\sin\alpha + \cos\phi\sin\gamma\cos\alpha]\mathrm{d}\phi \quad (2)$$

where $\varPhi$ is the corresponding surface angle when $\boldsymbol{n}$ and $\boldsymbol{n}'$ are orthogonal, that is

$$\varPhi = \arccos(-\tan\alpha/\tan\gamma) \quad (3)$$

Substituting (3) into (2) and simplifying further, $A_{proj}(R, \alpha, \gamma)$ can be rewritten as

$$A_{proj}(R,\alpha,\gamma) = A_{proj}(R,\alpha,\beta)\cdot(1 - \varPsi(\alpha,\beta)\cdot\theta\cos\omega_p t)$$
$$\varPsi(\alpha,\beta) = \frac{\sin\varPhi\cos\beta\cos\alpha - \varPhi\sin\beta\sin\alpha}{\sin\varPhi\sin\beta\cos\alpha + \varPhi\cos\beta\sin\alpha}.$$

However, the fundamental inertia axis $\boldsymbol{e}_z$ of RV is not generally consistent with its geometrical vertical axis due to the uneven distributed mass. The drift angle between them is approximately $0.5^\circ - 1^\circ$. As illustrated in Fig. 3, denoting this angle as φ, then $A_{proj}(R, \alpha, \gamma)$ would be similarly derived as

$$A_{proj}(R,\alpha,\gamma) = A_{proj}(R,\alpha,\beta)\cdot$$
$$(1 - \varPsi(\alpha,\beta)\cdot\theta\cos\omega_p t - \varPsi(\alpha,\beta)\cdot\varphi\cos\omega_s t) =$$
$$\overline{A}_{proj}(1 - \varPsi(\alpha,\beta)\cdot\theta\cos\omega_p t - \varPsi(\alpha,\beta)\cdot\varphi\cos\omega_s t). \quad (4)$$

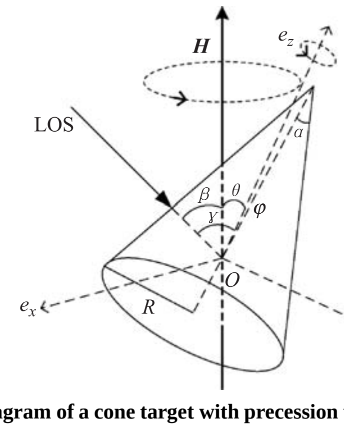

Fig. 3 Diagram of a cone target with precession when its inertia axis is inconsistent with geometrical vertical axis

2.2 Tumbling

Unlike precession motion, tumbling is just a single rotation without accompanying by another one [4]. Illustrated in Fig. 4 is a cone target tumbling around $\boldsymbol{H}$ with the angular velocity ω_t. The angle θ between the geometrical vertical axis and $\boldsymbol{H}$ is defined as tumbling angle. Similar to (1), the observation angle $\gamma(t)$ becomes

$$\gamma(t) = \arccos(\cos\theta\cos\beta + \cos\omega_t t\sin\theta\sin\beta). \quad (5)$$

Based on (2), (3) and (5), the projected area of tumbling target can be derived as

$$A_{proj}(R,\alpha,\gamma) =$$
$$\begin{cases} \pi r^2\cos\gamma, \quad \gamma\in[0,\alpha) \\ r^2\cos\gamma\arccos(-\tan\alpha/\tan\gamma) + \\ \qquad r^2/\sin\gamma\sqrt{\cos^2\alpha - \cos^2\gamma}, \quad \gamma\in[\alpha,\pi/2) \\ -r^2\cos\gamma\arccos(\tan\alpha/\tan\gamma) + \\ \qquad r^2/\sin\gamma\sqrt{\cos^2\alpha-\cos^2\gamma}, \quad \gamma\in[\pi/2,\pi-\alpha) \\ -\pi r^2\cos\gamma, \quad \gamma\in[\pi-\alpha,\pi) \end{cases}.$$

Generally the tumbling angle θ is close to 90°, so the range of $\gamma(t)$ would be relatively large. Therefore, projected area time series of tumbling target would present complex waveform structures. Because $\gamma(t)$ is periodic, $A_{proj}(R, \alpha, \gamma)$ is also periodic,

$$A_{proj}(R,\alpha,\gamma) = \overline{A}_{proj}(1 + a_t f(\omega_t t + \theta_t)) \quad (6)$$

where $f(\cdot)$ is the periodic function of the projected area, a_t denotes the corresponding amplitude coefficient, and θ_t is the initial phase.

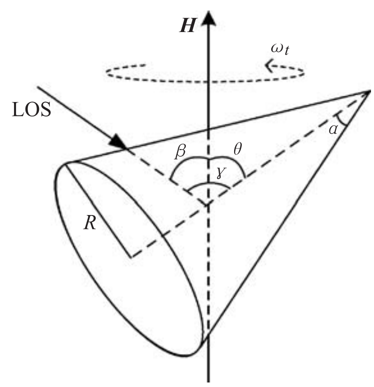

Fig. 4 Diagram of the cone target with tumbling

To sum up, the projected area of cone targets with precession or tumbling can be precisely formulated as mathematical formulas with the related parameter ω_p, ω_s, ω_t and θ, which will serve as vital theoretical basis to distinguish different types of micro-motions or estimate target parameters.

3. Extraction of periodic characteristics from IR signatures

According to Section 1, if target projected area time series can be decoupled from IR signatures, it is feasible to distinguish different types of micro-motions and estimate related parameters.

3.1 IR signatures modeling and simulating

Assuming ballistic targets have gray-body radiation and diffuse reflection properties, according to Planck's law, the radiation intensity through the detector aperture within the wavelength range $\lambda_1 - \lambda_2$ [2] is

$$I(\lambda_1 - \lambda_2) = A_0 A_{proj}/(\pi R^2)\int_{\lambda_1}^{\lambda_2} M(\lambda, T)\mathrm{d}\lambda \cdot \Delta t$$

where A_0 is the aperture area of the IR detector, $M(\lambda, T)$ is the radiation density, and Δt is the dwell time. If we subsume all the known variables in κ, the received irradiance intensity becomes

$$I(\lambda_1 - \lambda_2) = \kappa A_{proj} \cdot 1/R^2 \cdot u(T) \tag{7}$$

where T, R and A_{proj} are the time-varying variables: temperature of target surface, detecting distance, target projected area, and A_{proj} is a linear variable of the irradiance intensity.

According to (4) and (6), the IR irradiance intensity signature can be rewritten as

$$\begin{gathered} I_{prec}(t) = \\ \overline{I}(t) \cdot (1 - \varPsi(\alpha, \beta) \cdot \theta \cos\omega_p t - \varPsi(\alpha, \beta) \cdot \varphi \cos\omega_s t) \\ I_{tumb}(t) = \overline{I}(t) \cdot (1 + a_t f(\omega_t t + \theta_t)) \end{gathered} \tag{8}$$

where

$$\overline{I}(t) = \kappa \cdot \overline{A}_{proj} \cdot 1/R^2 \cdot u(T)$$

denotes the trend of IR signature induced by the decrease of detecting distance and the variation of temperature.

The state update of target micro-motions can be achieved by rotational matrices determined by Euler angles. Define $\boldsymbol{R}_x(\eta)$, $\boldsymbol{R}_y(\eta)$ and $\boldsymbol{R}_z(\eta)$ as rotating about x-axis, y-axis and z-axis with angle η respectively. Due to the target's rotation, each point on the target would move to a new position in the reference coordinate system, which can be achieved by multiplying a set of rotation matrices. For example, during the interval Δt, the mathematical relationship between the initial position vector $\boldsymbol{M}_1$ and the new position vector $\boldsymbol{M}_2$ can be represented as

$$\boldsymbol{M}_2 = \boldsymbol{R}_{prec}\boldsymbol{M}_1 = \boldsymbol{R}_Z(\omega_p\Delta t)\cdot\boldsymbol{R}_X(\theta)\cdot\boldsymbol{R}_Z(\omega_s\Delta t)\cdot\boldsymbol{M}_1$$

$$\boldsymbol{M}_2 = \boldsymbol{R}_{tumb}\boldsymbol{M}_1 = \boldsymbol{R}_Z(\omega_t\Delta t)\cdot\boldsymbol{R}_X(\theta)\cdot\boldsymbol{M}_1$$

The relative motions between the target and the IR detector are depicted in Fig. 5. Assuming that the direction of LOS does not change during the very short observed interval, the angle β is fixed. In the simulations, all of the motion parameters are set with respect to the Earth center Inertial Coordinates (EIC) [7]. Initial position, velocities and other stimulation parameters are predetermined as listed in Table 1. Assume the observed interval is 8 s and the scan rate is 100 Hz. The simulated target projected area time series and IR signatures with Gaussian white noise are displayed in Fig. 6 and Fig. 7 respectively. Note that SNR is defined as the ratio of the standard deviation of the signal to the one of noise, namely,

$$\mathrm{SNR} = \sigma_s/\sigma_n.$$

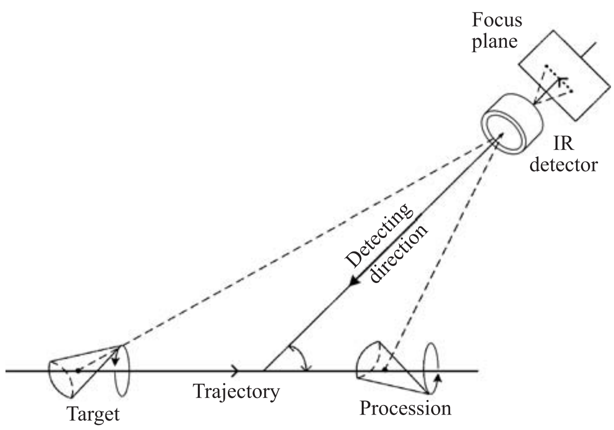

Fig. 5 Relative motion between the target and the detector

Table 1 Simulation parameters of the ballistic target and IR detector

Target structure	Shape	Size	3D model
	Flat-base cone (The geometrical axis is misaligned 1° with respect to its inertia axis)	Semi-vertical angle 10° Cone radius 0.2 m	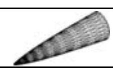
Irradiance parameter	Initial temperature	Temperature increment	Emissivity
	320 K	+0.1 K	0.3
Bulk-motion parameter	Initial position	Velocity	
	[−12e3, 0, 659 6e3]	[3e3,0,0]	
Micro-motion parameter	Procession motion	Tumbling	
	Spinning frequency 2.5 Hz Coning frequency 0.5 Hz Coning angle 3°	Tumbling frequency 0.5 Hz Tumbling angle 90°	
IR detector parameter	Lens aperture	Bands range	Spectrum transmittance
	0.138 m	8 – 12 μm	0.8

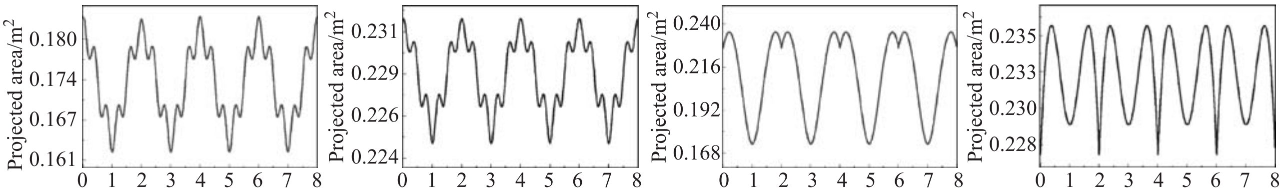

(a) Precession (β=30°, φ=1°) (b) Precession (β=60°, φ=1°) (c) Tumbing (β=30°) (d) Tumbing (β=60°)

Fig. 6 Projected area time series of a cone target with precession and tumbling

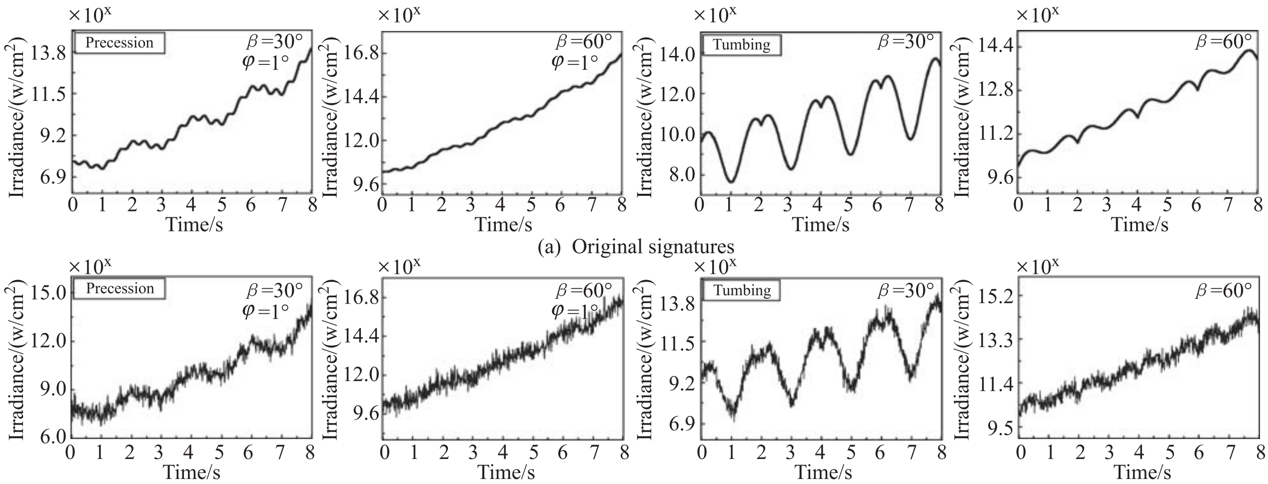

(a) Original signatures

(b) Noisy signatures with SNR of 6 dB

Fig. 7 IR simulation signatures of the targets with precession and tumbling

3.2 Periodic characteristics extracting

From Fig. 6 and Fig.7, we can draw the following conclusions: (i) Each IR signature presents an increasing trend accompanied by the periodic fluctuation, and the fluctuation amplitude becomes larger as time goes on. (ii) IR signatures have the same periodic characteristics with target projected area time series. This is because the time-varying variable $A_{proj}(t)$ is a linear factor to determine IR signatures. Based on the conclusions above, an IR signature with noise can be decomposed into several components, such as trend, periodic component and noise, namely,

$$\widetilde{I}(t) = Tr(t) + Pe(t) + \varepsilon$$

where $Tr(t)$ is the trend of the signature, and $Pe(t)$ is the periodic component, and ε is the noise. Referring to (8), we can deduce that, (take precession as an example)

$$Tr(t) = \overline{I}(t)$$

$$Pe(t) = -\overline{I}(t)\cdot(\varPsi(\alpha,\beta)\cdot\theta\cos\omega_p t + \varPsi(\alpha,\beta)\cdot\varphi\cos\omega_s t).$$

Define the periodic characteristic function as

$$a(t) = I(t)/Tr(t) =$$
$$1 - \varPsi(\alpha,\beta)\cdot\theta\cos\omega_p t - \varPsi(\alpha,\beta)\cdot\varphi\cos\omega_s t. \quad (9)$$

According to (9), if an IR signature is decomposed into trend and periodic component, the periodic characteristics $a(t)$ can be decoupled. From $a(t)$, parts of target parameters, including micro-motion parameters $\omega_p, \omega_s, \theta$ and semi-vertical angle α of cone targets, can be estimated.

To decompose IR signatures, the low-pass filtering or linear methods, which are unable to analyze the non-linear and non-stationary data, are not suitable. Inspired by the empirical mode decomposition method (EMD) [8], we offer an efficient method, called envelope mean method (EM), to extract trend and periodic component. For an IR signature with noise $x(t)$, EM has the following major steps:

Step 1 Initialize $i = 0$ and $x_i(t) = x(t)$.

Step 2 Extract the local minima and maxima of the IR signature. Using the extremes, the envelope E_{down} of the minima and the envelope E_{up} of the maxima are formed by cubic spline interpolation.

Step 3 Calculate the mean of these two envelopes as $m_i(t) = (E_{down} + E_{up})/2$ and let $x_{i+1}(t) = m_i(t)$.

Step 4 If the extreme number of $x_{i+1}(t)$ is less than two, then stop the algorithm and let $Tr(t) = x_{i+1}(t)$; otherwise, set $i = i + 1$ and skip back to Step 2.

However, the EM algorithm extracts the mean of the envelopes depending on all the extremes, which has poor performances under the strong noisy conditions. For that, we improve the algorithm by adding a certain intensity of white noise into the original signatures, performing n independent Monte-Carlo trials and averaging all the results. The experimental results are illustrated in Fig. 8.

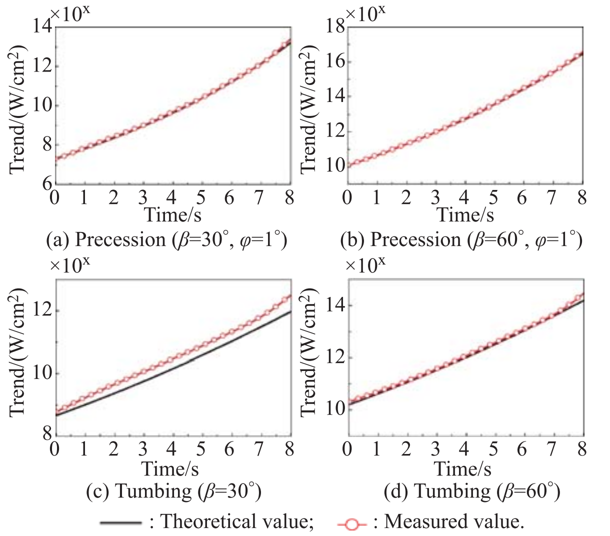

Fig. 8 Results of trend extracting from the noisy signatures with SNR of 6 dB

After extracting the trend and periodic component from the IR signature, according to (9), the noisy periodic characteristics function $\widetilde{a}(t)$ becomes

$$\widetilde{a}(t) = \widetilde{I}(t)/Tr(t) = a(t) + \varepsilon/Tr(t).$$

Considering the periodic and stationary properties of $\widetilde{a}(t)$, we introduce a de-noising method based on singular spectrum analysis (SSA) [9]. This method makes full use of the global data information and achieves good de-noised performance. The algorithm is detailed as follows.

Step 1 Extract the period M of input signature $\widetilde{a}(t)$. The time-domain autocorrelation method is an effective tool to estimate the period of noisy data [10]. This method cuts out a piece of signature $\widetilde{a}_l(t) = (\widetilde{a}_1, \dots, \widetilde{a}_l)$ from original signature $\widetilde{a}_N(t) = (\widetilde{a}_1, \dots, \widetilde{a}_N)$ and calculates the correlation coefficients between $\widetilde{a}_N(t)$ and $\widetilde{a}_l(t)$, which leads to an auto-correlation sequence of length $N - l + 1$. Only if $l > M$, the auto-correlation sequence would present several maxima at the locations $0, M+1, 2M+1, \cdots$.

Step 2 Transfer the signature $\widetilde{a}_L(t) = (\widetilde{a}_1, \dots, \widetilde{a}_L)$ into the multi-dimensional series set $x_1, \dots, x_L$ with the cycle-spinning operation on the signature. For example, $\boldsymbol{x}_1 = (\widetilde{a}_L, \widetilde{a}_1, \dots, \widetilde{a}_{L-1})^{\mathrm{T}}$, where L is a multiple of M and $L \leqslant N$. The result of this step is a trajectory matrix $\boldsymbol{X} = [\boldsymbol{x}_1, \dots, \boldsymbol{x}_L]$.

Step 3 Apply singular value decomposition (SVD) to decompose $\boldsymbol{X}$ into $\boldsymbol{X} = \boldsymbol{U}[\lambda_1, \dots, \lambda_L]\boldsymbol{V}^{\mathrm{T}}$, where $\lambda_1, \dots, \lambda_L$ are singulars of $\boldsymbol{X}$ in a decreasing order, and $\boldsymbol{U}$ and $\boldsymbol{V}$ are the corresponding left and right singular vectors respectively.

Step 4 Reconstruct the first $d(1 \leqslant d \leqslant L)$ singulars and split into $\boldsymbol{X}$ two components, the de-noised one and noise. The de-noised component is

$$\boldsymbol{X}_{deno} = \sum_{i=1}^{d} u_i \sigma_i \boldsymbol{v}_i^{\mathrm{T}}.$$

The de-noised signature $a(t)$ of $\widetilde{a}(t)$ is the first row vector of $\boldsymbol{X}_{deno}$. Ideally, the dimension d should be chosen such that $\lambda_d \gg \lambda_{d+1}$. The results obtained by our proposed de-noising method are illustrated in Fig. 9.

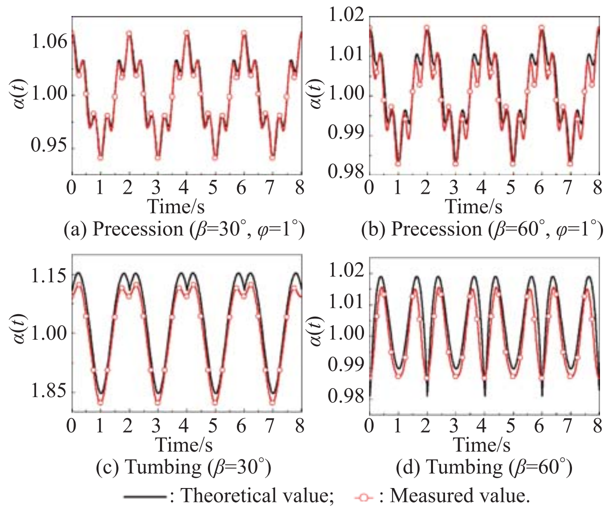

Fig. 9 Results of de-noised $a(t)$ extracting from the noisy data with SNR of 6 dB

4. Classification of micro-motion types and parameters estimation

By analyzing the periodic characteristics $a(t)$ decoupled from IR signatures, we would propose algorithms to distinguish different micro-motion types and estimate related parameters. Note that all the experiment data are from the simulation data based on the simulation parameters in Table 1.

4.1 Micro-motion types distinguishing

According to the definition of $a(t)$, the periodic characteristics of targets signatures with precession and tumbling can be expressed as

$$\begin{cases} a_p(t) = 1 - \Psi(\alpha, \beta) \cdot \theta \cos \omega_p t - \Psi(\alpha, \beta) \cdot \varphi \cos \omega_s t \\ a_t(t) = 1 + a_t f(\omega_t t + \theta_t) \end{cases}. \tag{10}$$

And from (10), it is known that $a_p(t)$ is approximately a pure sinusoidal function. Thus $a_p(t)$ has the property of half-period rotation symmetry. Namely, the first-half period of $a_p(t)$ undergoing a 180° rotation around the midpoint can coincide with the second-half. But $a_t(t)$ does not have the property of half-period rotation symmetry, because $a_t(t)$ is generally a complicated periodic function, as analyzed in Section 2. Therefore, we can identify different micro-motion types with reference to this criterion.

Concretely, defining $a^1_{M/2}$, $a^2_{M/2}$ as the first-half period and the second-half one of $a(t)$ respectively, then we assess the rotation symmetry of $a(t)$ by using root mean squared error (RMSE).

$$\text{REMS} = \sqrt{2/M \cdot \sum_i (a^1_{M/2}(i) - Rot(a^2_{M/2}(i)))^2}$$

where $Rot(\cdot)$ is the 180° rotation operation.

Recorded in Table 2 are the REMS of half-period rotation symmetry of IR signatures with different levels of noise. It is found that the REMS of $a_p(t)$ always stays in a lower level, about from 0.1e–3 to 4.0e–3. While, the REMS of $a_t(t)$ is higher than 7.0e–3 and stays at a relatively high level. Based on this criterion, the types of micro-motions would be distinguished.

Table 2 REMS of half-period rotation symmetry of target signatures with precession and tumbling 10^{-2}

SNR/dB	Precession $/a_p(t)$				Tumbling $/a_t(t)$			
	$\beta = 30^\circ$	$\beta = 40^\circ$	$\beta = 50^\circ$	$\beta = 60^\circ$	$\beta = 30^\circ$	$\beta = 40^\circ$	$\beta = 50^\circ$	$\beta = 60^\circ$
20	0.014 3	0.048 1	0.092 8	0.164 4	0.735 0	0.807 9	1.429 7	1.641 6
10	0.056 7	0.085 0	0.134 9	0.265 8	0.726 2	0.853 7	1.344 5	1.613 2
6	0.102 3	0.147 3	0.216 8	0.370 4	0.702 6	0.820 3	1.387 5	1.585 3

4.2 Parameters estimating

The estimated parameters include $\omega_p, \omega_s, \theta$ of precession and ω_t of tumbling. The values of ω_p and ω_t can be calculated by the period M of IR signatures. Thus, the rest of estimated parameters are ω_s, θ.

Considering that $a_p(t)$ is a pure sinusoidal function with two frequency components, we adopt the frequency spectrogram analysis technique to estimate the values of ω_s. Fig. 10 displays the single-sided amplitude spectrograms of $a_p(t)$ whose frequency resolution Δf is 0.125 Hz. Only if the drift angle φ is larger than 0°, the accurate value of ω_s can be estimated from the spectrogram. Typically θ is bigger than φ, so the amplitude at frequency ω_p is bigger than the amplitude at ω_s, which is the technique to distinguish ω_p and ω_s. For example in Fig. 10, the value ω_s is 2.5 Hz.

According to (10), if the parameters α and β are known, it is easy to estimate θ. In the practical missile defense, it is easy to calculate the value of β according to the motion velocity of IR detector and the projected positions of the target in the focus plane. For simplicity, the value of β is assumed to be known. Thus, the key of estimating θ lies on α.

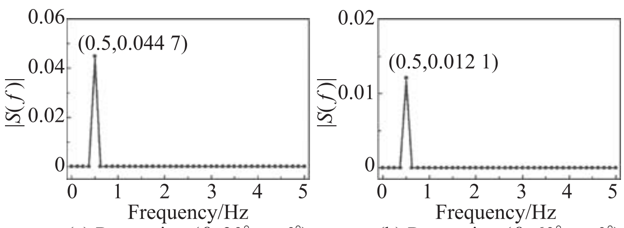

(a) Precession (β=30°, φ=0°) (b) Precession (β=60°, φ=0°)

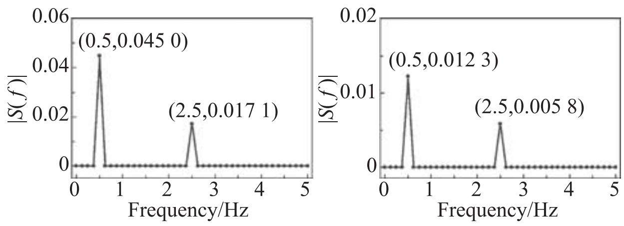

(c) Tumbing (β=30°, φ=1°) (d) Tumbing (β=60°, φ=1°)

Fig. 10 Single-sided amplitude spectrum of $a(t)$ from the data with SNR of 6 dB

If the value of α is known, the value of θ can be calculated based on the mathematical formulas in (10). As shown in Table 3, we present the estimated results of θ when β is 30°, 40°, 50° and 60°. According to the recorded data, the estimation precision of θ is up to 95% when SNR > 3, as shown in the bold area. Otherwise, the estimation performance is relatively poor, especially when β is 50° or 60°. This is because the periodic fluctuations of IR signatures are totally covered in the noise, and it is unable to decouple the periodic characteristics $a_p(t)$ from IR signature.

Table 3 Coning angle θ estimated in precession with the known α

SNR/dB	20	10	6	3	2
$\beta = 30^\circ$	**2.995**	**3.019**	**3.056**	**3.148**	3.251
$\beta = 40^\circ$	**2.985**	**3.020**	**3.068**	**3.189**	3.328
$\beta = 50^\circ$	**2.974**	**3.029**	**3.092**	3.267	3.460
$\beta = 60^\circ$	**2.963**	**3.052**	**3.168**	3.474	3.802

If the value of α is unknown, we cannot estimate θ by utilizing just one data example. Considering that the detector changes its observation angle β every once a while, we would obtain a plenty of data examples during the whole intercepting process. By constructing simultaneous equations of two data examples, we can calculate both values of α and θ according to (10). In the estimation experiments, we arbitrarily choose two data examples as a set to jointly estimate α and θ. According to the results recorded in Table 4, the estimation accuracy is generally guaranteed by using our method under the high SNR conditions, e.g. SNR >3 dB.

Table 4 Coning angle θ estimated in precession when α is unknown

SNR/dB	10		6		3	
	$\alpha/(^\circ)$	$\theta/(^\circ)$	$\alpha/(^\circ)$	$\theta/(^\circ)$	$\alpha/(^\circ)$	$\theta/(^\circ)$
$\beta = 30^\circ\&35^\circ$	10.17	3.063	10.26	3.116	11.16	3.439
$\beta = 40^\circ\&45^\circ$	9.99	3.016	9.36	2.916	8.48	2.861
$\beta = 50^\circ\&55^\circ$	9.63	2.927	9.54	2.971	8.37	2.846
$\beta = 30^\circ\&40^\circ$	10.08	3.041	10.71	3.236	12.42	3.853
$\beta = 40^\circ\&50^\circ$	9.99	3.017	9.36	2.916	8.49	2.865
$\beta = 50^\circ\&60^\circ$	9.81	2.973	9.45	2.948	8.28	2.826

By analyzing the results from Tables 2 – 4, we can draw the following conclusions:

(i) When θ is small, it is feasible to distinguish different micro-motion types based on the principle of half-period rotation symmetry. The periodic characteristics function $a_p(t)$ of IR signatures with precession satisfies the symmetry condition, but $a_t(t)$ of tumbling does not.

(ii) When the prior parameter β is known, the micro-motion parameters can be estimated with reference to (10). Especially, under the high SNR condition (SNR > 3 dB), the estimation precision of θ is up to 95%. Meanwhile, by constructing simultaneous equations of two data examples, we can accurately calculate the value of θ, even if α is unknown.

5. Conclusions

In this paper, we investigate ways of extracting the micro-motion dynamic features of ballistic midcourse targets from the signals of IR detection. The main idea is to distinguish micro-motion types and estimate micro-motion parameters by analyzing the periodic fluctuation characteristic of IR signatures. Experiments have verified that under the low-noise conditions (SNR > 3 dB), it is feasible to distinguish micro-motion types and estimate related parameters using our proposed methods. Moreover, the research ideas are applied to the cone targets, and also to the targets with other shapes. Our research results would provide important references for ballistic midcourse targets recognition.

References

[1] W. Zhang, K. Li, W. Jiang. Parameter estimation of radar targets with macro-motion and micro-motion based on circular correlation coefficients. *IEEE Signal Processing Letters*, 2015, 22(4): 633 – 637.

[2] C. Z. Qiu, Z. Y. Zhang, H. Z. Lu, et al. Infrared modeling and imaging simulation of midcourse ballistic targets based on strap-down platform. *Journal of Systems Engineering and Electronics*, 2014, 25(4): 776 – 785.

[3] L. Ma. The micro-motion characteristic and combining classification of ballistic target. Changsha, China: National University of Defense Technology, 2011.

[4] V. C. Chen, F. Li, S. Ho, et al. Micro-Doppler effect in radar: phenomenon, model, and simulation study. *IEEE Trans. on Aerospace and Electronic Systems*, 2006, 42: 2 – 21.

[5] D. J. Feng, J. Liu, M. Dan. RCS period analysis and estimation of ballistic midcourse targets. *Journal of Astronautics*, 2008, 29(1): 362 – 365.

[6] X. L. Sun, W. Hou, X. L. Liu. Small infrared target detection using frequency-spatial cues in a single image. *Journal of Electronic Imaging*, 2014, 23(4): 1 – 10.

[7] R. W. Zhang. *Satellite orbit attitude dynamics and control*. Beijing: Beihang University Press, 1998.

[8] D. P. Fairchild, R. M. Narayanan. Classification of human motions using empirical mode decomposition of human micro-Doppler signatures. *IET Radar, Sonar and Navigation*, 2014, 8(4): 425 – 434.

[9] H. Hossein. Singular spectrum analysis: methodology and comparison. *Journal of Data Science*, 2007, 5: 239 – 257.

[10] J. Niu, K. L. Li, W. D. Jiang, et al. A new method of micro-motion parameters estimation based on cyclic autocorrelation function. *Science China: Information Sciences*, 2013, 56: 1 – 11.

Biographies

Junliang Liu was born in 1988. He received his M.S. degree in science and technology of electronic information from National University of Defense Technology (NUDT), Changsha, China, in 2013. He is currently a Ph. D. candidate at the Laboratory of Automatic Target Recognition, NUDT. His research interests include optical guidance, target recognition and signal processing.
E-mail: liujunliang_1988@163.com

Yanfang Li was born in 1986. She received her B.S. and M.S. degrees in optical information science and technology from Beijing Jiaotong University, Beijing, China, in 2007 and 2011 respectively. She is currently an engineer with Beijing Institute of Remote Sensing Equipment. Her research interests include photoelectric imaging, target detection, system design and image processing.
E-mail: sxsz_lyf@126.com

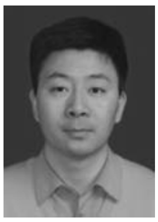

Shangfeng Chen was born in 1978. He received his M.S. and Ph.D. degrees from NUDT, Changsha, China, in 2004 and 2009 respectively. He is currently a lecturer at Laboratory of Automatic Target Recognition, NUDT. His research interests include automatic target recognition and real time system.
E-mail: cactus510@sina.com

Huanzhang Lu was born in 1963. He received his M.S. and Ph.D. degrees from NUDT, Changsha, China, in 1990 and 1994 respectively. He is currently a full professor at Laboratory of Automatic Target Recognition, NUDT. His research interests include automatic target recognition, precision and real time system.
E-mail: luhz@nudt.edu.cn

Bendong Zhao was born in 1992. He received his B.S. degree from NUDT, Changsha, China, in 2013. He is currently a Ph. D. candidate at the Laboratory of Automatic Target Recognition, NUDT. His research interests include infrared target recognition, machine learning and pattern recognition.
E-mail: zhaobendong_nudt@163.com